UC San Diego

UC San Diego Previously Published Works

Title

Intrinsic evolution of the decoupling and coupling of the plasma density and temperature in a cylindrical laboratory plasma device

Permalink

https://escholarship.org/uc/item/8352w9q3

Journal

Physics of Plasmas, 30(6)

ISSN

1070-664X

Authors

Wang, CY

Xiao, WW

Ren, Y

et al.

Publication Date

2023-06-01

DOI

10.1063/5.0146229

Peer reviewed

eScholarship.org Powered by the California Digital Library
University of California

Physics of Plasmas

RESEARCH ARTICLE | JUNE 07 2023

Intrinsic evolution of the decoupling and coupling of the plasma density and temperature in a cylindrical laboratory plasma device

Special Collection: Turbulence in Plasmas and Fluids

C. Y. Wang; W. W. Xiao ; Y. Ren ; P. H. Diamond ; X. B. Peng; J. T. Ma ; W. J. Zhong

Check for updates

Physics of Plasmas 30, 062303 (2023)
https://doi.org/10.1063/5.0146229

View Online
Export Citation
CrossMark

Downloaded from http://pubs.aip.org/aip/pop/article-pdf/doi/10.1063/5.0146229/17978951/062303_1_5.0146229.pdf

AIP Publishing

Physics of Plasmas ARTICLE pubs.aip.org/aip/pop

Intrinsic evolution of the decoupling and coupling of the plasma density and temperature in a cylindrical laboratory plasma device

Cite as: Phys. Plasmas **30**, 062303 (2023); doi: 10.1063/5.0146229
Submitted: 11 February 2023 · Accepted: 19 May 2023 ·
Published Online: 7 June 2023

View Online Export Citation CrossMark

C. Y. Wang,[1] W. W. Xiao,[1,a)] Y. Ren,[2] P. H. Diamond,[3] X. B. Peng,[4] J. T. Ma,[1] and W. J. Zhong[1]

AFFILIATIONS

[1]Institute for Fusion Theory and Simulation, School of Physics, Zhejiang University, Hangzhou 310027, China
[2]PPPL, Princeton University, P. O. Box 451, Princeton, New Jersey 08543, USA
[3]Center for Energy Research, University of California San Diego, La Jolla, California 92093, USA
[4]Institute of Plasma Physics, Chinese Academy of Sciences, Hefei, Anhui 230031, China

Note: This paper is part of the special topic, Turbulence in Plasmas and Fluids.
[a)]**Author to whom correspondence should be addressed:** wwxiao@zju.edu.cn

ABSTRACT

An intrinsic evolution in the decoupling–coupling–decoupling (DCD) of the electron density and temperature responding to the magnetic field change is observed in a cylindrical laboratory plasma device. Experimental results show that the density and the temperature decouple in the low magnetic field, couple with higher magnetic field, and decouple again with a continuous magnetic field increase. An element physical picture of the DCD regime is unraveled based on the analyses of gradient lengths, the turbulence propagation directions, the turbulence spatial scales, and the relationship between the normalized collision rates and the poloidal mode numbers.

Published under an exclusive license by AIP Publishing. https://doi.org/10.1063/5.0146229

I. INTRODUCTION

Since sawtooth oscillation was first observed[1] in the magnetically confinement fusion (MCF) field, the physics of the coupling and decoupling has been studied for several decades.[2–6] The coupling and the decoupling between the density profiles and the temperature are extensive and important physical phenomena in magnetized plasma. Typically, the density profiles and the temperature profiles are generally reported on the high confinement mode (H-mode)[7–9] and the improved energy confinement mode (I-mode)[10–13] in the tokamak edge region.

In this work, we report an intrinsic evolution of the decoupling–coupling–decoupling (DCD) based on the gradient changes of the density and the temperature in the Zheda Plasma Experimental Device (ZPED). Here, the "coupling" means that the gradients of the density and the temperature change synchronously; the "decoupling" means that the density gradient and the temperature gradient change asynchronously or reversely change. The distinct physics in the intrinsic evolution of the decoupling and coupling of the plasma density and temperature was discussed from three aspects in this paper. First, the temperature gradient almost does not change, while the density gradient increases with the magnetic field increase from 0.5 to 0.8 kGs. This means that the decoupling phenomenon exists due to the asynchronous change of the gradients in region I. Then, the density gradient and the temperature gradient synchronously increase with the magnetic field increase from 0.8 to 1.1 kGs. This is so-called the coupling phenomenon in region II. Then, the density gradient almost does not change, while the temperature gradient continuously increases with the magnetic field increase from 1.1 to 2 kGs. We call the density and the temperature are decoupled in region III. Second, the propagation directions of the poloidal wavenumber (k_θ) and the radial wavenumber (k_r) with magnetic field change, and the drift wave (DW)[14] extends to a higher frequency region. Third, the density gradients drive a nonlinear change of the density fluctuations with the magnetic field increase, and the integral density decreases, but the integral temperature increases. Meanwhile, the relationship between the normalized collision rates of the electron to electron (ν_{ee}^*) and the poloidal mode numbers (m) at $r = 4.5$ cm is strongly related to the density. This means that one potential mechanism affects density, which is the driven source of the DCD regime in this experiment. Finally, we discussed the H-mode and I-mode plasmas on the ν_{ee}^* and the m based on a few tokamak experiments. A comparison shows that the intrinsic evolution of the DCD phenomenon is similar to the edge

Downloaded from http://pubs.aip.org/aip/pop/article-pdf/doi/10.1063/5.0146229/17978951/062303_1_5.0146229.pdf

Published under an exclusive license by AIP Publishing

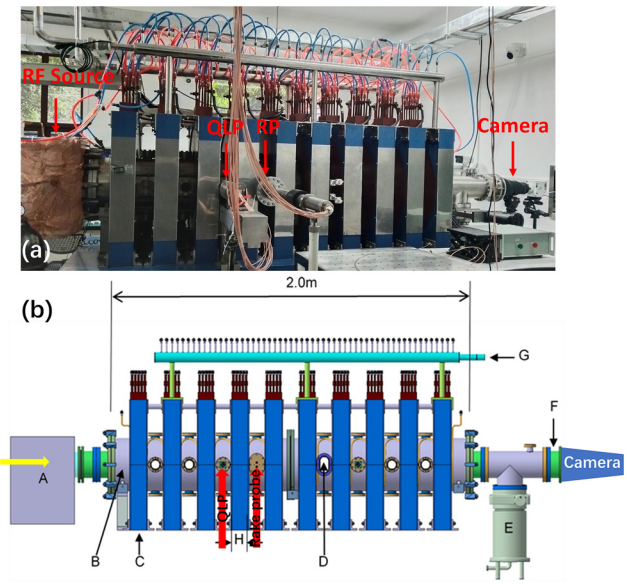

FIG. 1. (a) is the real device picture and (b) is the schematic diagram of the ZPED.[17] The locations of the Quadruple Langmuir probe (QLP) and the Langmuir rake probes are marked by the red arrows. A camera is localized at the end of the device for the observation of the poloidal mode numbers (m).

gradient changes between the H-mode and the I-mode plasmas. The density could be one of the key parameters associated with the transfer between the H-mode and I-mode.

II. EXPERIMENT SETUP

The experiments reported were carried on the Zheda Plasma Experimental Device (ZPED),[15] which is a cylindrical magnetized plasma device at Zhejiang University, as shown in Fig. 1. Figure 1(a) is the picture of the real device, and Fig. 1(b) is the schematic diagram of the ZPED. The size of the vacuum chamber is 2.0 m in length and 0.3 m in diameter. The nitrogen plasma is produced by a 13.56 MHz radio frequency (RF) source with about 200 W forward and about 20 W reflect power. The *A* to the *G* represent the RF source, the vacuum chamber, the magnetic coils, the diagnostic window for the microwave reflectometry, the throttle valve and pump system, the glass observation window, and the cooling water tubes, respectively. The coil thick is 94 mm as shown in Fig. 1(b-H). The gas fueling system is located at the head of the vacuum chamber, as shown by the yellow arrow. The Quadruple Langmuir probe (QLP)[16] and the Langmuir rake probes are the key diagnostics for the density and temperature profiles and the density fluctuations in this experiment. The sampling frequency of the QLP and the Langmuir rake Langmuir probes is 2 MHz. The locations of the QLP and the Langmuir rake probes are marked by the red arrows in Figs. 1(a) and 1(b). A camera is localized at the end of the device for the observation of the poloidal mode numbers (m).

The detailed structures and directions of the QLP and the Langmuir rake probes are shown in Fig. 2. The diagram of QLP is shown in Fig. 2(a). It consists of four tungsten tips: 1, 2, 3, and 4 of 1 cm in length and 1.4 mm in diameter. The distance between the tip3 and the tip4 along the poloidal direction is 4.6 mm, and the distance between the tip1 and tip2 along the magnetic field direction is 4.5 mm, as shown in Fig. 2(a). The plasma profiles (electron density, electron temperature), the density fluctuations, and the poloidal wavenumbers (k_θ) are measured by the QLP. The diagram of the Langmuir rake probe is shown in Fig. 2(b). It consists of 12 tungsten tips in the radial direction from the center to the edge. The length and the diameter of each tip are 2 and 2 mm, respectively. The distance between two adjacent tips is 4 mm. The radial wavenumbers (k_r) can be measured by the Langmuir rake probe. The magnetic field direction and the moving direction of the QLP and the Langmuir rake probe are marked by the arrows in Fig. 2. In the experiment, a passive RF compensation circuit is connected just after the probe tip. The detailed parameters of each probe tip are the capacitance is 20 pF and the inductance is 6.8 μH. The main purpose of the RF compensation circuit is to eliminate the influence of the 13.56 MHz RF signal from the RF source.[18] In this work, all of the poloidal mode numbers (m) can be observed by the fast camera diagnostic, which includes a high-speed camera and a lens system, as shown in Fig. 1. The camera parameters are the spatial resolution of 512 × 512, frames per second of 24 000, and the exposure time of 10 μs. The details on the fast camera diagnostic were studied in Ref. 19.

III. EXPERIMENTAL RESULTS AND ANALYSIS

A. The measurements of the density and the temperature

The density profiles and the temperature profiles with different magnetic fields are measured by the QLP as shown in Figs. 3(a) and 3(b),

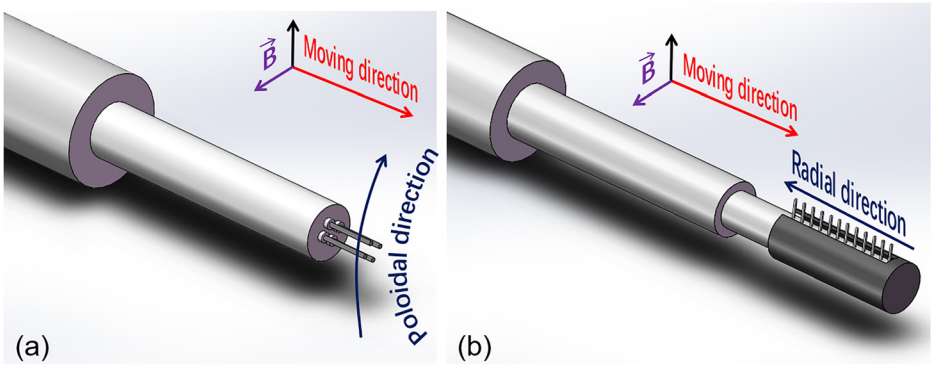

FIG. 2. (a) is the diagram of QLP and (b) is the diagram of the Langmuir rake probe. The magnetic field direction, the poloidal direction, and the moving direction are indicated by the arrows.

Downloaded from http://pubs.aip.org/aip/pop/article-pdf/doi/10.1063/5.0146229/17978951/062303_1_5.0146229.pdf

Published under an exclusive license by AIP Publishing

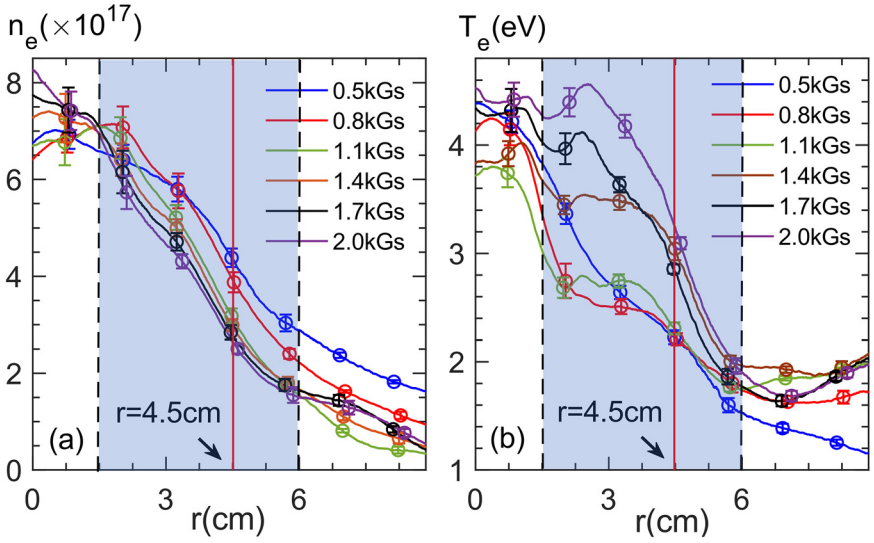

FIG. 3. (a) and (b) are the density profiles and the temperature profiles, respectively. The main analysis region is at r = 4.5 cm, as shown by the red line. The regions of the integral density and the integral temperature are represented by the shaded bars, which are confirmed by the black dashed lines. Corresponding to the integral density and the integral temperature will be discussed in Sec. III D.

respectively. Actually, in order to measure the profiles of the density and the temperature, we used the reciprocating motion method to get the raw data. It means that the QLP system is driven by an electric motor, which is controlled by the software as experiment needed, such as the swept velocity and the depth in the plasma. In Fig. 3, the numbers of each global profile of the density and the temperature are about 2×10^5 along the radial direction, and the representative points with the error bars on the profiles are to avoid the curves of the profiles overlap each other.

However, the ionization of the gas in the linear machine is a non-negligible issue because there is no extra heating source except the RF source. Thus, the plasma temperature decreases from the head to the rear of the device. In order to get good plasma performance on the ZPED, the optimized detection positions of the QLP and the Langmuir rake probe are considered to avoid the RF source influence and the plasma temperature drop. The distance between the RF source and the probes is about 80–100 cm, as shown in Fig. 1 by the red arrows. In addition, we chose a special region of the plasma, as shown in Fig. 3 by the shaded bars. The turbulence and the incomplete ionization in the plasma edge are the main reasons for the measurement errors of the Langmuir probe system. Meanwhile, in the core region of the linear machine, the hollow profiles of the density and temperature are often observed in linear machines, a possibility is also the incomplete ionization in the core region of a linear device. Thus, we chose the special region to study, as shown in Fig. 3 by the shaded bars.

A local ionization of the gas is estimated using the Saha equation[20,21] $a^2/(1-a^2) = (2.4 \times 10^{-4}/p)T^{2.5}e^{-u/KT}$. The main analysis region of the local ionization of the gas is at r ~4.5 cm (as shown by the red lines in Fig. 3). Then, the local ionization of the gas could be estimated. The local ionization number a is about 99% at the local measurement position only, r ~4.5 cm. Here, the T represents the thermodynamic temperature, ~3×10^4 K; the ionization energy (u) of the nitrogen atom is 14.5 eV; the plasma temperature (KT) is about 3 eV; and the pressure (p) is about 1.5 mTorr, which was measured by the vacuum gauge in the ZPED. Note: the local ionization of the gas does not imply the global ionization because the recombination rate of the electron–ion will increase as long as it is far from the RF source in a linear machine without an extra heating source, and the global ionization of low-temperature plasma using the Saha equation should be studied based on more special experiments or using a coronal model estimate for the globe ionization balance due to the complex atomic molecular physics processes.

B. The density gradient evolution with different magnetic fields

Based on Fig. 3, a detailed analysis of the gradient is shown in Fig. 4. The density gradient length ($1/L_{ne} = \Delta n_e/n_e$) and the temperature gradient length ($1/L_{Te} = \Delta T_e/T_e$) are shown by the blue curve and the red curve, respectively. The density gradient increases with the magnetic field increase, while the temperature gradient almost does

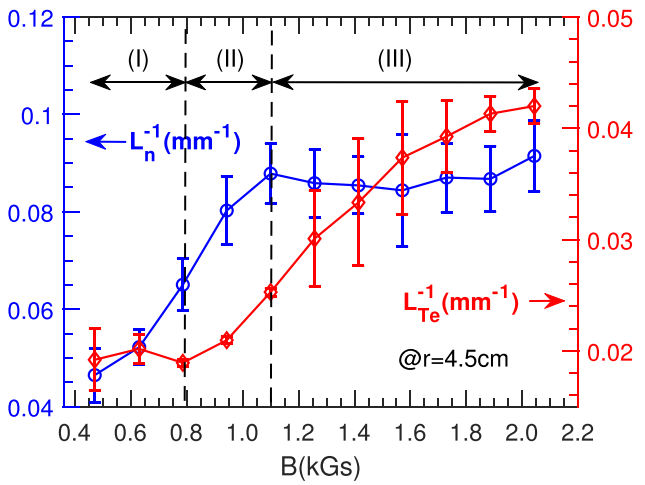

FIG. 4. The distributions of the $1/L_n$ and the $1/L_{Te}$ at r = 4.5 cm with magnetic field change. The three regions of the DCD regime are separated by the gradient changes of the density and the temperature.

Downloaded from http://pubs.aip.org/aip/pop/article-pdf/doi/10.1063/5.0146229/17978951/062303_1_5.0146229.pdf

Published under an exclusive license by AIP Publishing

not change even the magnetic fields increase, as shown in Fig. 4 in region I. The density gradient continuously increases, meanwhile the temperature gradient increases with the magnetic increase as well in region II; however, the temperature gradient increases with the magnetic field increase, but the density gradient almost does not change in region III. These results indicate that the DCD regime exists with the magnetic field increase:

(1) the density profile and the temperature profile are decoupled in region I, and density gradient increases while the temperature gradient almost does not change;
(2) the density and the temperature are coupled in region II, and both the density gradient and the temperature gradient increase synergistically;
(3) the density and the temperature are decoupled, and the temperature gradient increases while the density gradient does not change in region III.

C. The analysis of the wavenumber spectra and the density fluctuation

In each region, the fundamental physics of the DCD regime related to the wavenumber spectra, and the density fluctuation are analyzed, as shown in Fig. 5. The poloidal and the radial wavenumber spectra are obtained according to the two-point correlation method,[22,23] and the cross power spectra of floating voltage measured by two floating probes are derived with $C^j_{XY} = X^j(f)Y^{j^*}(f) = Ae^{j\cdot\theta_j(f)}$, where j is the number of samples, X and Y are the Fourier transform of floating voltage, and the star "$*$" denotes the complex conjugation. The wavenumber k_j is confirmed by the phase difference θ_j, $k_j(f) = \theta_j(f)/\Delta d$. By sum up complex amplitude of different samples, wavenumber spectra $S(k,f)$ can be calculated, $S(k,f) = \frac{1}{M}\sum_{j=1}^{M} I_{(0,\Delta k)} \times [k - k^j(f)] \cdot |C^j_{XY}(f)|$. Thus, the wavenumber–frequency spectra S(k, f) of potential fluctuations for radial position r = 4.5 cm in regions I, II, and III are shown in Fig. 5. Here, the (a), (b), and (c) represent the changes of the poloidal wavenumber (k_θ) in regions I, II, and III; the (d), (e), and (f) represent the changes of the radial wavenumber (k_r) in regions I, II, and III.

In region I: in Figs. 5(a) and 5(d), the m = 1 at 0.5 kGs, the k_θ is at ion diamagnetic direction (i-direction, the turbulence spatial scale $k_\theta\rho_S = k_\theta\frac{\sqrt{m_iT_e}}{eB} = k_\theta\frac{\sqrt{14\times1.66\times10^{-27}\times1.6\times10^{-19}T_e(\mathrm{eV})}}{1.6\times10^{-19}\cdot B} = 3.8\times10^{-4}\frac{k_\theta\sqrt{T_e(eV)}}{B} = 0.69$, B = 0.5 kGs, $|k_\theta| < 60\,\mathrm{m}^{-1}$, $T_e \approx 2.3$ eV, $\rho_S = 0.0116$ m), while the k_r is outward as shown in Fig. 5(d), and the frequency of the DW turbulence is below 10 kHz, as shown in Figs. 5(a) and 5(d) by the blue dashed lines.

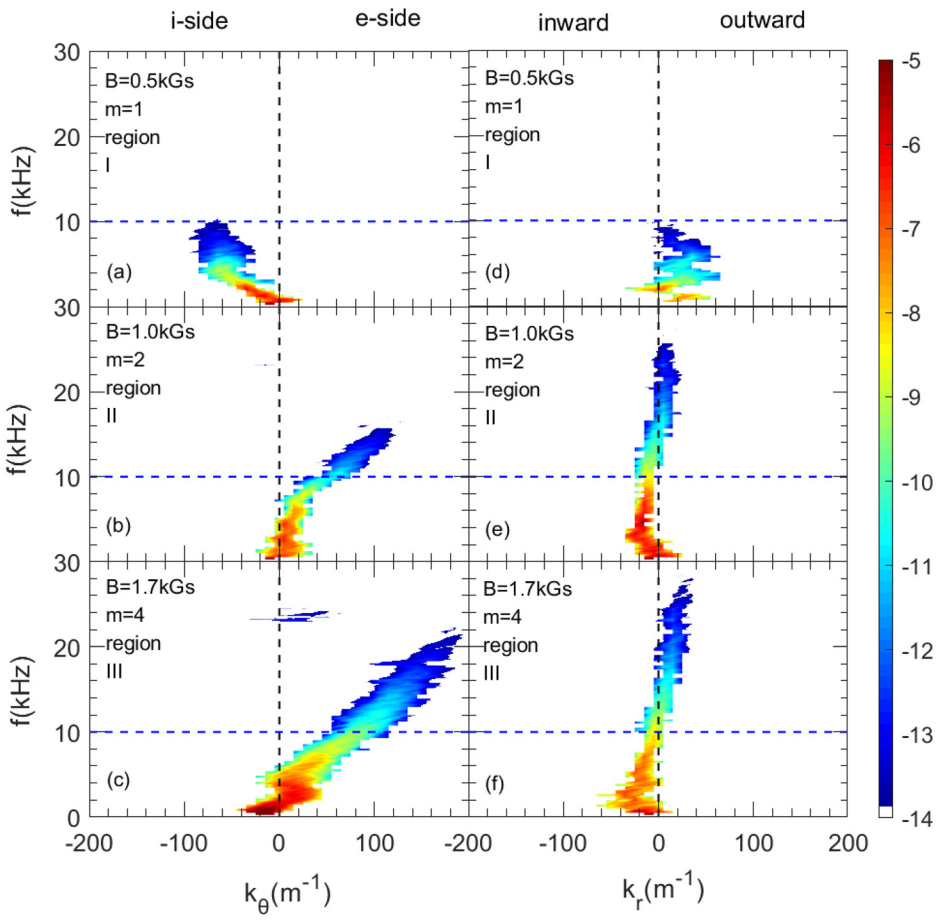

FIG. 5. Wavenumber–frequency spectra S(k, f) of the density fluctuations at r = 4.5 cm in regions I, II, and III. Here, the (a), (b), and (c) are the S(k_θ, f); the (d), (e), and (f) are the S(k_r, f).

Downloaded from http://pubs.aip.org/aip/pop/article-pdf/doi/10.1063/5.0146229/17978951/062303_1_5.0146229.pdf

Published under an exclusive license by AIP Publishing

In region II: in Figs. 5(b) and 5(e), the m increases to 2 at 1.0 kGs, while the k_θ is at the electron diamagnetic direction (e-direction, the turbulence scale $k_\theta \rho_S = 0.5904 < 0.6$, B = 1000 Gs, $|k_\theta| < 110\ \mathrm{m}^{-1}$, $T_e \approx 2.4$ eV, $\rho_S = 0.0054$ m), while the k_r is outward as shown in Fig. 5(e), and the frequency of the DW turbulence expands to a higher frequency range as shown in Figs. 5(b) and 5(d).

In region III: when the magnetic field continuously increases, the m increases to 4 at 1.7 kGs, the DW turbulence gradually transfers from ion diamagnetic direction to the electron diamagnetic direction, and the absolute value of wavenumbers is much larger than that in regions I and II, as shown in Fig. 5(c). While, the k_r indicates that the turbulence transport in the low-frequency region is still inward, but the higher frequency turbulence transport is outward much, as shown in Fig. 5(f).

These results suggest that the low-frequency turbulence dominantly exists in low magnetic field. The turbulence propagation is at the ion diamagnetic direction. This is useful for the density increase since the diamagnetic effects as a finite pressure fluctuation to increase the total Reynolds force significantly.[17] While, with the magnetic field increase, the poloidal mode numbers increase from m = 1 to m = 4. It is clear that the turbulence frequency expands to a higher frequency and the turbulence propagation direction gradually reverses from i-side to e-side, as shown in Figs. 5(b) and 5(c). The radial wavenumber spectra $S(k_r, f)$ suggest that the turbulence frequency also increases, and the low-frequency component of the turbulence is outward, as shown in Fig. 5(d). In Figs. 5(e) and 5(f), the higher frequency component of the turbulence is outward and the low-frequency component of the turbulence reverses to inward direction. These results indicate that the drift wave turbulence with higher frequency could dominantly affect the particle confinement.[24,25] The drift wave turbulence with higher frequency was driven by the magnetic field rising, as shown in Figs. 5(c) and 5(f). The particle confinement degradation is presented by the integral density decrease with the magnetic field increase, as shown in Fig. 6(b).

Note: there is no clear difference between regions II and III except the drift wave frequency increase. This indicates that there may be a coexisting status of the turbulence types from region II to region III. Actually, it is a little bit difficult to clearly separate the turbulence scales, the transport channels, and the stabilization mechanisms.[26] Thus, it is better to specify the dominant characteristics in each region. Especially, in region III, the drift wave turbulence expands with the magnetic field increase and induces the confinement degradation. This is consistent with the drift wave turbulences that occur universally in magnetized plasmas producing the dominant mechanism for the transport of particles.[27]

D. The ν^*_{ee} vs to the m

The turbulence saturation can be observed at the steep density gradient region when the magnetic field exceeds a critical magnetic field,[28] which is defined due to the knee point of the density fluctuation curve, as shown in Fig. 6(a) by the blue dashed line. Here, the fluctuation amplitude of the density is calculated from 4 to 20 kHz at r = 4.5 cm, corresponding to the steep density gradient region in Fig. 3 by the red line. An integral density and temperature with different magnetic fields are also calculated, as shown in Fig. 6(b). The integral regions are presented in Figs. 3(a) and 3(b) by the black dashed lines, from r = 1.5 to 6 cm in the ZPED. One can see that the integral density

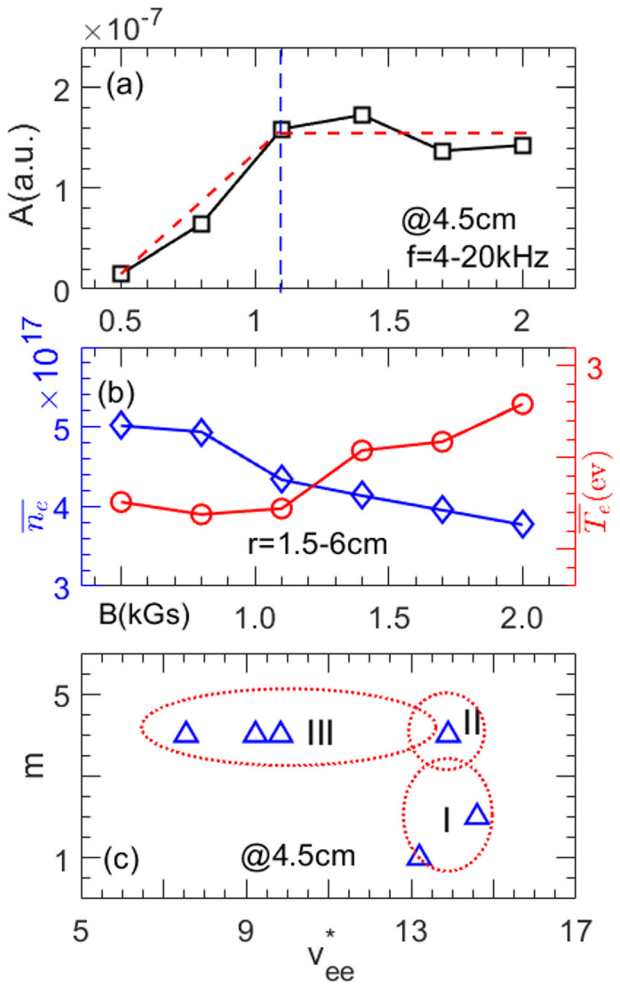

FIG. 6. (a) is the amplitudes of the density fluctuation with different magnetic fields, and the critical magnetic field is pointed by the blue dashed line. (b) shows the integral density and the integral temperature, and the integral radius r is from 1.5 to 6 cm. (c) represents the relationship between the ν^*_{ee} and the m.

decreases, but the temperature increases with the magnetic field increase with no external particle, heating, and momentum source. A possible reason is that the magnetic field leads to the increase of the DW turbulence amplitude and reduces the particle confinement until to the turbulence amplitude saturation[29] in region III. This is consistent with the results in Fig. 6(b), the particle confinement dissipation with the increase of the DW turbulence; conversely, the temperature increases with the magnetic field increase. It suggests that an intrinsic evolution of the decoupling transport channel exists between the density and the temperature in a Cylindrical Laboratory Plasma Device with the magnetic field increase.

Thus, a relationship of the ν^*_{ee} vs to the m is studied for a deep understanding of the intrinsic evolution of the DCD regime in this work, as shown in Fig. 6(c). The ν^*_{ee} related to the m at r = 4.5 cm is calculated by the $\nu^*_{ee} = \nu/\omega_p$, $\omega_p = \sqrt{\frac{4\pi n_e e^2}{m_e}}$ as shown in Fig. 6(c).[30] Here, the ν^*_{ee} is the normalized collision rate of the electron to electron,

Downloaded from http://pubs.aip.org/aip/pop/article-pdf/doi/10.1063/5.0146229/17978951/062303_1_5.0146229.pdf

Published under an exclusive license by AIP Publishing

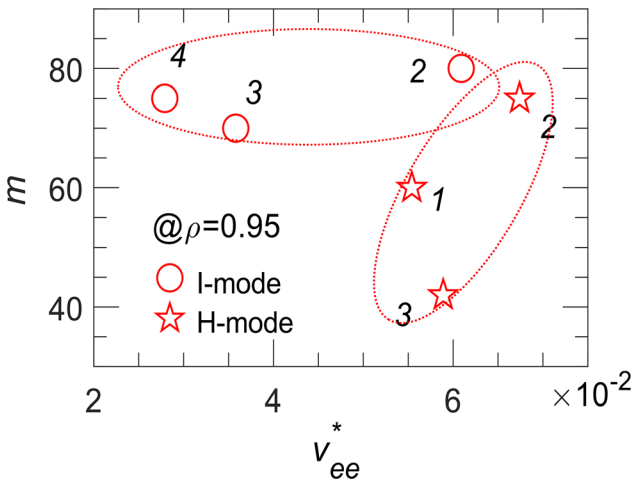

FIG. 7. The relationship between the v_{ee}^* and the m. The numbers 1–4 correspond to the data from the tokamaks DIII-D, EAST, ASDEX-U, and C-MOD. The red stars and the red circles represent the H-mode and the I-mode plasmas with different densities, respectively. The details are shown in Table I.

ν is the collision rate by the $\nu = 2.91 \times 10^{-6} n_e \ln\Lambda T_e^{-3/2} s^{-1}$ and the $\ln\Lambda = 23 - \ln(n_e^{\frac{1}{2}} T_e^{-\frac{3}{2}})$ at $T_e \leq 10$ eV, the ω_p is the plasma frequency, the n_e is the plasma density, the e is the electronic charge, and the m_e is the electron mass, respectively. A change trend of the v_{ee}^* vs to the m in the three regions is shown in Fig. 6(c) by the dotted ellipses. The v_{ee}^* does not change while the m increases in Fig. 6(c) region I, the m stops increasing in Fig. 6(c) in region II, the m is almost saturated, and the v_{ee}^* decreases in Fig. 6(c) region III. These suggest that the low density due to the turbulence dissipation is one of the key points of the intrinsic evolution on the DCD regime of the density and the temperature.

IV. DISCUSSION AND SUMMARY

Actually, a few typical results on the v_{ee}^* vs the m related to the H-mode and I-mode plasmas from different machines are statistically evaluated in the plasma edge region at $\rho = 0.95$, as shown in Fig. 7. The data points are based on the experimental results from DIII-D, EAST, ASDEX-U, and C-MOD. The red stars and the red circles represent the H-mode and the I-mode plasmas with different densities, respectively. Table I shows the v_{ee}^*, the m, and the $\langle n_e \rangle$. It is clear that the H-mode plasma density is larger than that in the I-mode case based on the data in Table I. A regular shape of the v_{ee}^* vs to the m is almost similar to the results in Fig. 6(c). A comparison between Fig. 7 and Fig. 6(c) indicates that the density is a key parameter to induce the intrinsic evolution of the DCD regime, and this may be helpful to understand the different transport channels of the density and the temperature in the H-mode and the I-mode plasmas.[31]

TABLE I. The details of the $v_{ee}^*(\times 10^{-2})$, m, and $\langle n_e \rangle (\times 10^{19}\,\mathrm{m}^{-3})$ from a few tokamaks with H-mode and I-mode plasmas.

		DIII-D	EAST	ASDEX-U	C-MOD
v_{ee}^*	H	5.54[31]	6.74[32]	2.83[31,33]	5.89[31]
	I	7.34[31]	6.09[34]	2.79[31,33]	3.58[12,31]
m	H	60[35]	75[36–38]	40[39,40]	42[41,42]
	I	∼70[12,43]	∼75[34]	75[44]	∼70[12]
$\langle n_e \rangle$	H	5.5[45]	3[37]	∼5.0[46,47]	∼26[48]
	I	4.5[12]	∼2.5[38]	∼3.5[33]	∼12[49]

In general, an intrinsic evolution on the DCD regime has been observed on ZPED with the magnetic field increase: first, the temperature gradient almost did not change, while the density gradient increased in region I, and this phenomenon is called decoupling between the density and the temperature; second, both density and temperature gradient increased synergistically in region II, and this phenomenon is called coupling between the density and the temperature; third, the density gradient almost did not change, while the temperature gradient continuously increased with the magnetic field increase in region III, and this is called decoupling again between the density and the temperature. In addition, with the magnetic field increase, the turbulence propagation direction gradually reversed, and the DW turbulence frequency expanded to a higher frequency region with a higher wavenumber. The DW turbulence dominantly reduced the density and degraded particle confinement, which is the element point to change the density. A regular shape of the v_{ee}^* vs to the m identifies that the density is a key parameter of the intrinsic evolution on the DCD regime in the cylindrical laboratory plasma.

How to confirm a global plasma ionization in a linear machine with about 5 eV and a density less than 10^{18} m^{-3} could be a new direction to study; even the Saha equation might be applied to explain a local ionization in low-temperature plasma in this paper. However, this conclusion of the local ionization using Saha is possible as a reference only.[50,51] Thus, it would be more appropriate to use a coronal model estimate for the ionization balance in the linear machine plasma. A valuable research direction on this point will be focused in the next experimental studies.

ACKNOWLEDGMENTS

The authors thank J. Q. Dong, X. T. Ding, G. R. Tynan, and X. L. Zou for many enlightening discussions. This work was supported by the National Natural Science Foundation of China (Grant No. 11875234) and the National Magnetic Confinement Fusion Science Program of China (Nos. 2017YFE0301206, 2017YFE0300500, and 2017YFE0301200).

AUTHOR DECLARATIONS

Conflict of Interest

The authors have no conflicts to disclose.

Author Contributions

Chiyu Wang: Data curation (equal); Formal analysis (equal); Funding acquisition (equal); Software (equal); Writing – original draft (equal). **Weiwen Xiao:** Conceptualization (equal); Data curation (equal); Formal analysis (equal); Funding acquisition (equal); Investigation (equal); Project administration (equal); Resources (equal); Supervision (equal); Writing – review & editing (equal). **Yang Ren:** Investigation (supporting). **Patrick Diamond:** Investigation (supporting). **X. B. Peng:** Investigation (supporting). **Jiatong Ma:** Data curation (supporting). **Wenjie Zhong:** Data curation (supporting).

Downloaded from http://pubs.aip.org/aip/pop/article-pdf/doi/10.1063/5.0146229/17978951/062303_1_5.0146229.pdf

Published under an exclusive license by AIP Publishing

DATA AVAILABILITY

The data that support the findings of this study are available from the corresponding author upon reasonable request.

REFERENCES

[1]J. D. Callen and G. L. Jahns, "Experimental measurement of electron heat diffusivity in a tokamak," Phys. Rev. Lett. **38**, 491–494 (1977).
[2]D. L. Brower, C. X. Yu, R. V. Bravenec, H. Lin, N. C. Luhmann, W. A. Peebles, C. P. Ritz, B. A. Smith, A. J. Wootton, Z. M. Zhang, and S. J. Zhao, "Confinement degradation and enhanced microturbulence as longtime precursors to high-density-limit tokamak disruptions," Phys. Rev. Lett. **67**, 200–203 (1991).
[3]G. M. D. Hogeweij, J. O'Rourke, and A. C. C. Sips, "Evidence of coupling of thermal and particle transport from heat and density pulse measurements in jet," Plasma Phys. Controlled Fusion **33**, 189 (1991).
[4]N. Deliyanakis, D. P. O'Brien, B. Balet, C. M. Greenfield, L. Porte, A. C. C. Sips, P. M. Stubberfield, and H. Wilson, "The VH-mode at JET," Plasma Phys. Controlled Fusion **36**, 1159 (1994).
[5]C. Hidalgo, B. Gonçalves, C. Silva, M. A. Pedrosa, K. Erents, M. Hron, and G. F. Matthews, "Experimental investigation of dynamical coupling between turbulent transport and parallel flows in the jet plasma-boundary region," Phys. Rev. Lett. **91**, 065001 (2003).
[6]G. R. Tynan, R. A. Moyer, M. J. Burin, and C. Holland, "On the nonlinear turbulent dynamics of shear-flow decorrelation and zonal flow generation," Phys. Plasmas **8**, 2691–2699 (2001).
[7]F. Wagner, G. Fussmann, T. Grave, M. Keilhacker, M. Kornherr, K. Lackner, K. McCormick, E. R. Müller, A. Stäbler, G. Becker, K. Bernhardi, U. Ditte, A. Eberhagen, O. Gehre, J. Gernhardt, G. v Gierke, E. Glock, O. Gruber, G. Haas, M. Hesse, G. Janeschitz, F. Karger, S. Kissel, O. Klüber, G. Lisitano, H. M. Mayer, D. Meisel, V. Mertens, H. Murmann, W. Poschenrieder, H. Rapp, H. Röhr, F. Ryter, F. Schneider, G. Siller, P. Smeulders, F. Söldner, E. Speth, K. H. Steuer, Z. Szymanski, and O. Vollmer, "Development of an edge transport barrier at the h-mode transition of ASDEX," Phys. Rev. Lett. **53**, 1453–1456 (1984).
[8]D. P. Schissel, M. A. Mahdavi, J. C. DeBoo, and M. Le, "Decoupling the effects of plasma current and plasma density on DIII-D H mode energy confinement," Nucl. Fusion **34**, 1401 (1994).
[9]D. G. Whyte, A. E. Hubbard, J. W. Hughes, B. Lipschultz, J. E. Rice, E. S. Marmar, M. Greenwald, I. Cziegler, A. Dominguez, T. Golfinopoulos, N. Howard, L. Lin, R. M. McDermott, M. Porkolab, M. L. Reinke, J. Terry, N. Tsujii, S. Wolfe, S. Wukitch, Y. Lin, and Alcator C-Mod Team, "I-mode: An H-mode energy confinement regime with L-mode particle transport in Alcator C-Mod," Nucl. Fusion **50**, 105005 (2010).
[10]A. Hubbard, D. Whyte, R. Churchill, I. Cziegler, A. Dominguez, T. Golfinopoulos, J. Hughes, J. Rice, M. Greenwald, N. Howard, B. Lipschultz, E. Marmar, M. Reinke, J. Terry, I. Bespamyatnov, and W. Rowan, "Edge energy transport barrier and turbulence in the I-mode regime on Alcator C-Mod," Phys. Plasmas **18**, 056115 (2011).
[11]T. Happel, P. Manz, F. Ryter, M. Bernert, M. Dunne, P. Hennequin, A. Hetzenecker, U. Stroth, G. D. Conway, L. Guimarais, C. Honoré, E. Viezzer, and ASDEX Upgrade Team, "The I-mode confinement regime at ASDEX Upgrade: Global properties and characterization of strongly intermittent density fluctuations," Plasma Phys. Controlled Fusion **59**, 014004 (2016).
[12]A. Marinoni, J. C. Rost, M. Porkolab, A. E. Hubbard, T. H. Osborne, A. E. White, D. G. Whyte, T. L. Rhodes, E. M. Davis, D. R. Ernst, K. H. Burrell, and DIII-D Team, "Characterization of density fluctuations during the search for an I-mode regime on the DIII-D tokamak," Nucl. Fusion **55**, 093019 (2015).
[13]A. E. White, P. Phillips, D. G. Whyte, A. E. Hubbard, C. Sung, J. W. Hughes, A. Dominguez, J. Terry, and I. Cziegler, "Electron temperature fluctuations associated with the weakly coherent mode in the edge of I-mode plasmas," Nucl. Fusion **51**, 113005 (2011).
[14]P. H. Diamond, A. Hasegawa, and K. Mima, "Vorticity dynamics, drift wave turbulence, and zonal flows: A look back and a look ahead," Plasma Phys. Controlled Fusion **53**, 124001 (2011).
[15]W. W. Xiao, C. Y. Wang, J. X. Zhu, N. Wali, K. Wang, Z. M. Sheng, and G. Y. Fu, "Observation of a nonlinear phenomenon of the density fluctuations on zheda plasma experiment device (ZPED)," AIP Adv. **9**, 075026 (2019).
[16]R. L. Burton, S. G. DelMedico, and J. C. Andrews, "Application of a quadruple probe technique to MPD thruster plume measurements," J. Propul. Power **9**, 771–777 (1993).
[17]A. I. Smolyakov, P. H. Diamond, and M. V. Medvedev, "Role of ion diamagnetic effects in the generation of large scale flows in toroidal ion temperature gradient mode turbulence," Phys. Plasmas **7**, 3987–3992 (2000).
[18]S. Ghosh, P. K. Chattopadhyay, J. Ghosh, and D. Bora, "RF compensation of single Langmuir probe in low density helicon plasma," Fusion Eng. Des. **112**, 915–918 (2016).
[19]J. T. Ma, W. W. Xiao, C. Y. Wang, N. Wali, and W. J. Zhong, "Plasma response associated with external magnetic perturbation fields in a cylindrical laboratory plasma device," Phys. Plasmas (unpublished) (2023).
[20]M. N. Saha, "LIII. Ionization in the solar chromosphere," London, Edinburgh, Dublin Philos. Mag. J. Sci. **40**, 472–488 (1920).
[21]M. N. Saha, "Versuch einer Theorie der physikalischen Erscheinungen bei hohen Temperaturen mit Anwendungen auf die Astrophysik," Z. Phys. **6**, 40–55 (1921).
[22]S. J. Levinson, J. M. Beall, E. J. Powers, and R. D. Bengtson, "Space/time statistics of the turbulence in a tokamak edge plasma," Nucl. Fusion **24**, 527 (1984).
[23]Y. Ren, W. Guttenfelder, S. Kaye, E. Mazzucato, R. Bell, A. Diallo, C. Domier, B. LeBlanc, K. Lee, M. Podesta, D. Smith, and H. Yuh, "Electron-scale turbulence spectra and plasma thermal transport responding to continuous $E \times B$ shear ramp-up in a spherical tokamak," Nucl. Fusion **53**, 083007 (2013).
[24]Z. Yan, G. R. McKee, R. Fonck, P. Gohil, R. J. Groebner, and T. H. Osborne, "Observation of the L-H confinement bifurcation triggered by a turbulence-driven shear flow in a tokamak plasma," Phys. Rev. Lett. **112**, 125002 (2014).
[25]C. Riccardi, D. Xuantong, M. Salierno, L. Gamberale, and M. Fontanesi, "Experimental analysis of drift waves destabilization in a toroidal plasma," Phys. Plasmas **4**, 3749–3758 (1997).
[26]T. Gorler and F. Jenko, "Scale separation between electron and ion thermal transport," Phys. Rev. Lett. **100**, 185002 (2008).
[27]W. Horton, "Drift waves and transport," Rev. Mod. Phys. **71**, 735–778 (1999).
[28]F. Halpern and P. Ricci, "Velocity shear, turbulent saturation, and steep plasma gradients in the scrape-off layer of inner-wall limited tokamaks," Nucl. Fusion **57**, 034001 (2016).
[29]P. H. Diamond, S.-I. Itoh, K. Itoh, and T. S. Hahm, "Zonal flows in plasma review," Rev. Sci. Instrum. **47**, R35 (2005).
[30]A. V. Latyshev and A. A. Yushkanov, "Behavior of a plasma with the collision rate proportional to the electron velocity in an external electric field," Theor. Math. Phys. **153**, 1697–1708 (2007).
[31]A. Hubbard, T. Osborne, F. Ryter, M. Austin, L. B. Orte, R. Churchill, I. Cziegler, M. Fenstermacher, R. Fischer, S. Gerhardt, R. Groebner, P. Gohil, T. Happel, J. Hughes, A. Loarte, R. Maingi, P. Manz, A. Marinoni, E. Marmar, R. McDermott, G. McKee, T. Rhodes, J. Rice, L. Schmitz, C. Theiler, E. Viezzer, J. Walk, A. White, D. Whyte, S. Wolfe, E. Wolfrum, Z. Yan, Alcator C-Mod, ASDEX Upgrade, and DIII-D Teams, "Multi-device studies of pedestal physics and confinement in the I-mode regime," Nucl. Fusion **56**, 086003 (2016).
[32]H. Wang, G. Xu, H. Guo, B. Wan, N. Yan, S. Ding, R. Chen, W. Zhang, L. Wang, S. Liu, L. Shao, L. Chen, Y. Liu, Y. Li, G. Hu, and N. Zhao, "Observation of a quasi-coherent high-frequency electromagnetic mode at the pedestal region in EAST RF-dominant H-modes," Nucl. Fusion **54**, 043014 (2014).
[33]F. Ryter, R. Fischer, J. Fuchs, T. Happel, R. McDermott, E. Viezzer, E. Wolfrum, L. B. Orte, M. Bernert, A. Burckhart, S. da Graça, B. Kurzan, P. McCarthy, T. Pütterich, W. Suttrop, M. Willensdorfer, and ASDEX Upgrade Team, "I-mode studies at ASDEX upgrade: L-I and I-H transitions, pedestal and confinement properties," Nucl. Fusion **57**, 016004 (2016).
[34]X. Feng, A. Liu, C. Zhou, Z. Liu, M. Wang, G. Zhuang, X. Zou, T. Wang, Y. Zhang, J. Xie, H. Liu, T. Zhang, Y. Liu, Y. Duan, L. Hu, G. Hu, D. Kong, S. Wang, H. Zhao, Y. Li, L. Shao, T. Xia, W. Ding, T. Lan, H. Li, W. Mao, W. Liu, X. Gao, J. Li, S. Zhang, X. Zhang, Z. Liu, C. Qu, S. Zhang, J. Zhang, J. Ji, H. Fan, and X. Zhong, "I-mode investigation on the experimental advanced superconducting tokamak," Nucl. Fusion **59**, 096025 (2019).
[35]I. Holod, D. Fulton, and Z. Lin, "Microturbulence in DIII-D tokamak pedestal. II. Electromagnetic instabilities," Nucl. Fusion **55**, 093020 (2015).

Downloaded from http://pubs.aip.org/aip/pop/article-pdf/doi/10.1063/5.0146229/17978951/062303_1_5.0146229.pdf

Published under an exclusive license by AIP Publishing

[36]H.-H. Wang, Y.-W. Sun, T.-H. Shi, S. Gu, Y.-Q. Liu, Q. Ma, Q. Zang, K.-Y. He, J.-P. Qian, B. Shen, D.-L. Chen, N. Chu, M.-N. Jia, J. Ren, Z.-P. Luo, Q.-P. Yuan, Y. Wang, B.-J. Xiao, Z.-C. Sheng, M.-H. Li, X.-Z. Gong, L. Zeng, and EAST Contributors, "Toroidal field and q_{95} scalings on error field penetration in EAST," Nucl. Fusion **60**, 126008 (2020).
[37]X. Z. Gong, B. N. Wan, J. G. Li, J. P. Qian, E. Z. Li, F. K. Liu, Y. P. Zhao, M. Wang, H. D. Xu, A. M. Garofalo, A. Ekedah, S. Y. Ding, J. Huang, L. Zhang, Q. Zang, H. Q. Liu, L. Zeng, S. Y. Lin, B. Shen, B. Zhang, L. M. Shao, B. J. Xiao, J. S. Hu, C. D. Hu, L. Q. Hu, L. Wang, Y. W. Sun, G. S. Xu, Y. F. Liang, N. Xiang, and EAST Team, Plasma Sci. Technol. **19**, 032001 (2017).
[38]Y. Liu, Z. Liu, A. Liu, C. Zhou, X. Feng, Y. Yang, T. Zhang, T. Xia, H. Liu, M. Wu, X. Zou, D. Kong, H. Li, J. Xie, T. Lan, W. Mao, S. Zhang, W. Ding, G. Zhuang, and W. Liu, "Power threshold and confinement of the I-mode in the EAST tokamak," Nucl. Fusion **60**, 082003 (2020).
[39]S. Kumar, K. Gopal, and D. N. Gupta, "Proton acceleration from overdense plasma target interacting with shaped laser pulses in the presence of pre-plasmas," Rev. Sci. Instrum. **61**, 085001 (2019).
[40]C. Maggi, R. Groebner, N. Oyama, R. Sartori, L. Horton, A. Sips, W. Suttrop, A. Leonard, T. Luce, M. Wade, Y. Kamada, H. Urano, Y. Andrew, C. Giroud, E. Joffrin, E. de la Luna, EFDA-JET Contributors for the Pedestal and Edge Physics, and Steady State Operation Topical Groups of the ITPA, "Characteristics of the H-mode pedestal in improved confinement scenarios in ASDEX upgrade, DIII-D, JET and JT-60U," Nucl. Fusion **47**, 535 (2007).
[41]Y. Huang, T. Xia, X. Xu, D. Kong, Y. Wang, Y. Ye, Z. Qian, Q. Zang, M. Wu, Y. Chu, H. Liu, B. Gui, X. Xiao, and D. Zhang, "Nonlinear simulation and energy analysis of the EAST coherent mode," Nucl. Fusion **60**, 026014 (2020).
[42]T. Golfinopoulos, B. LaBombard, D. Brunner, J. Terry, S. Baek, P. Ennever, E. Edlund, W. Han, W. Burke, S. Wolfe, J. Irby, J. Hughes, E. Fitzgerald, R. Granetz, M. Greenwald, R. Leccacorvi, E. Marmar, S. Pierson, M. Porkolab, R. Vieira, S. Wukitch, and Alcator C-Mod Team, "Edge transport and mode structure of a QCM-like fluctuation driven by the Shoelace antenna," Nucl. Fusion **58**, 056018 (2018).
[43]L. Schmitz, G. Wang, J. C. Hillesheim, T. L. Rhodes, W. A. Peebles, A. E. White, L. Zeng, T. A. Carter, and W. Solomon, "Detection of zonal flow spectra in DIII-D by a dual-channel Doppler backscattering system," Rev. Sci. Instrum. **79**, 10F113 (2008).
[44]P. Manz, T. Happel, F. Ryter, M. Bernert, G. Birkenmeier, G. Conway, M. Dunne, L. Guimarais, P. Hennequin, A. Hetzenecker, C. Honoré, P. Lauber, M. Maraschek, V. Nikolaeva, D. Prisiazhniuk, U. Stroth, E. Viezzer, and ASDEX Upgrade Team, "Turbulence characteristics of the I-mode confinement regime in ASDEX upgrade," Nucl. Fusion **57**, 086022 (2017).
[45]S. R. Haskey, A. Ashourvan, S. Banerjee, K. Barada, E. A. Belli, A. Bortolon, J. Candy, J. Chen, C. Chrystal, B. A. Grierson, R. J. Groebner, F. M. Laggner, M. Knolker, G. J. Kramer, M. R. Major, G. Mckee, G. M. Staebler, Z. Yan, and M. A. Van Zeeland, "Ion thermal transport in the H-mode edge transport barrier on DIII-D," Phys. Plasmas **29**, 012506 (2022).
[46]U. Plank, T. Pütterich, C. Angioni, M. Cavedon, G. D. Conway, R. Fischer, T. Happel, A. Kappatou, R. M. McDermott, P. A. Schneider, G. Tardini, M. Weiland, and A. U. team, "H-mode power threshold studies in mixed ion species plasmas at ASDEX upgrade," Nucl. Fusion **60**, 074001 (2020).
[47]F. Ryter, S. Rathgeber, L. B. Orte, M. Bernert, G. Conway, R. Fischer, T. Happel, B. Kurzan, R. McDermott, A. Scarabosio, W. Suttrop, E. Viezzer, M. Willensdorfer, E. Wolfrum, and ASDEX Upgrade Team, "Survey of the H-mode power threshold and transition physics studies in ASDEX upgrade," Nucl. Fusion **53**, 113003 (2013).
[48]A. Loarte, J. W. Hughes, M. L. Reinke, J. L. Terry, B. LaBombard, D. Brunner, M. Greenwald, B. Lipschultz, Y. Ma, S. Wukitch, and S. Wolfe, "High confinement/high radiated power H-mode experiments in Alcator C-Mod and consequences for International Thermonuclear Experimental Reactor (ITER) $Q_{DT} = 10$ operation," Phys. Plasmas **18**, 056105 (2011).
[49]M. Reinke, D. Brunner, T. Golfinopoulos, A. Hubbard, J. Hughes, A. Kuang, B. LaBombard, E. Marmar, R. Mumgaard, J. Terry, J. Lore, J. Canik, and I. Cziegler, and Alcator C-Mod Team, "Radiative heat exhaust in Alcator C-Mod I-Mode plasmas," Nucl. Fusion **59**, 046018 (2019).
[50]H. J. Kunze, *Introduction to Plasma Spectroscopy*, 1st ed. (Springer, Berlin/Heidelberg, 2009).
[51]I. H. Hutchinson, *Principles of Plasma Diagnostics*, 2nd ed. (Cambridge University Press, 2002).

Downloaded from http://pubs.aip.org/aip/pop/article-pdf/doi/10.1063/5.0146229/17978951/062303_1_5.0146229.pdf

Published under an exclusive license by AIP Publishing